# Additive Manufactured Open Cell Polyhedral Structures as Substrates for Automotive Catalysts

V. Papetti[1*], P. Dimopoulos Eggenschwiler[1], A. della Torre[2], F. Lucci[1**], A. Ortona[3], G. Montenegro[2]

[1] Laboratory for I.C. Engines, Empa, Swiss Federal Laboratories for Materials Testing and Research, Dübendorf, Switzerland
[2] Dipartimento di Energia, Politecnico di Milano, Milano, Italy
[3] HM Laboratory at MEMTI, SUPSI, Manno, Switzerland

* Corresponding author.
E-mail address:
viola.papetti@empa.ch
(V. Papetti).
** Present address: Philip Morris Products S.A., Research and Development, Switzerland.

**Abstract**
Polyhedral open cell lattice catalyst substrates are proposed based on results of numerical simulations and recent advances in Additive Manufacturing (AM) techniques.
Detailed simulations have compared different polyhedral structures in terms of mass transfer (aiming at optimal reactivity in the mass transfer limited domain) and flow through resistance. The simulations have taken into account dimensional limits given by the possibilities of AM techniques. Comparisons with state of art honeycombs have been also used in order to identify the optimal shape.
Substrates with these optimal characteristics have been manufactured out of $Al_2O_3$ with Stereolithography. Subsequently, these substrates have been coated and used for measurements of $C_3H_6$ oxidation in a model gas reactor. Measurements have focused in determining oxidation efficiency at different gas hourly space velocities as well as light-off behaviour.
Simulation results show that the optimal open cell structures are comprised by a cubic elementary cell rotated by 45° so that one spatial diagonal of the cube is aligned to the main gas flow. Higher porosities and smaller strut diameters improve the reactivity to pressure drop trade off. However, given the current manufacturing limitations, it is not possible to produce structures with strut diameters lower than 0.5 mm. This results in high porosity but low specific surface area (i.e $\varepsilon$=0.95 and $S_V$=400$m^2/m^3$). Thus, reaching a target conversion requires higher overall catalyst volume. The simulations show that for a series of geometrical parameters the open cell structures can reach identical conversion in respect to the honeycombs with only a fraction of the overall surface area and thus a fraction of the noble metals, while the overall dimensions are in the same order of magnitude and the pressure drop can reach lower levels.
Measurements in the model gas reactor confirm the mass transfer advantages of the polyhedral structures as predicted by the simulations. Measurements also show that the polyhedral lattices have very similar light-off behaviour in spite the four times lower surface area.

**Nomenclature**

| | |
|---|---|
| A: | Cross section of catalyst |
| AM: | Additive Manufacturing |
| CPSI: | Cells Per Square Inch, commercial characterization of honeycomb catalyst substrates |
| Cubic: | Additive Manufactured (AM) catalyst substrate consisting of cubes as elementary cells aligned with the main flow |
| Cubic45: | AM catalyst substrate consisting of cubes as elementary cells rotated by 45° so that one spatial diagonal of the cube is aligned to the main gas flow |
| $D_{ij}$: | Diffusivity of specie i in a gas j |
| $d_c$: | Wetted width of a (square) honeycomb channel |
| $D_c$: | Inner width of a (square) honeycomb channel, difference to $d_c$ is the coating thickness |
| $d_s$: | Strut diameter |
| ghsv: | Gas hourly space velocity through the catalyst, it corresponds to the ratio between the gas volume flow rate and the catalyst volume |
| HC: | Honeycomb catalyst substrate (conventional) |
| K: | Mass transfer coefficient |

| | |
|---|---|
| Kelvin: | AM catalyst substrate consisting of Kelvin cells (tetrakaidekahedral) as elementary cells |
| L: | Length of entire catalyst |
| $L_c$: | Cell length |
| $L_{s:}$ | Strut length (in case of Cubic elementary cells $L_c = L_s$) |
| $MM_i$: | Molar mass of specie i |
| $MM_{CH4}$: | Molar mass of methane |
| Octet: | AM catalyst substrate consisting of octets as elementary cells |
| PGM: | Platin Group Metalls |
| $\dot{Q}_{in}$: | Gas volume flow to the catalyst |
| rc: | Chamfer dimension at the corner in the HC structure |
| Re: | Reynolds number based on strut diameter |
| Sc: | Schmidt number |
| Sh: | Sherwood number |
| $S_v$: | Specific surface area |
| $S_w$: | Wetted surface area |
| SLA: | Stereo Lithography (additive manufacturing technique) |
| TC: | Thermo Couple |
| V: | Volume of entire catalyst |
| $v_{in}$: | Mean gas velocity upstream the catalyst entrance |
| $X_{CH4}$: | mass concentration of methane |
| Xi: | mass concentration of specie i |
| $Y_i$: | molar concentration of specie i |
| $Y_{CH4}$: | molar concentration of methane |
| $\Delta P$: | Pressure drop through the catalyst |
| ε: | (Macro-) Porosity of the catalyst |
| η: | Conversion through the catalyst |
| φ: | Tube quartz reactor diameter |

**Keywords**: Automotive Catalysts Open Cell Polyhedral Lattices, Additive Manufacturing, Honeycombs, Heat and Mass transfer in Catalysts, Catalyst Numerical Simulations, Model Gas Reactor.

## 1. INTRODUCTION

Catalyst technologies for automotive aftertreatment systems require constant developments to comply with the latest regulations concerning real driving emissions.

The current benchmark in catalyst substrates are honeycombs (HCs), while open cell structures represent a new paradigm that is gaining attention because of its promising properties [1]. In HCs the laminar flow in the channels results in low heat and mass transfer. Instead, the network of solid struts of the open cell lattices is characterized by tortuous paths that enhance gas-wall interactions and contribute to lower thermal inertia [2]. The result is higher conversion efficiencies [3][4], lower cold start emissions and higher flow uniformity, which is a key factor for catalyst durability [5][6][7][8]. They also allow more flexibility in the geometrical configuration of the reactor [9]. The increased mass and momentum transfer properties of open cell structures, however, result also in a higher pressure drop per unit of length [10][11], decreasing engine efficiency. Thus, to have a fair comparison, the performance index I has been introduced [3], which evaluates catalyst efficiency by relating conversion to pressure drop. CFD analysis suggested that the trade off is in favour of open cell structures when the porosity is high enough [1][12].

In the past, work on open cell catalysts focused on foam structures, with some degree of uncontrollable randomness, characterized by statistical averaged quantities [13]. Some effort has been spent on their modelling. Computing capabilities have allowed performing computational analysis of real CT foam scans [2][14][15][16][17]. Foams can also be accurately reconstructed with elaborated algorithms based on Voronoi tessellations [18][19][20]. However, these techniques increase the computational load. To simplify the procedure, in literature, an alternative has been to model foams as regular cell structures. Some works have been conducted by numerical simulations of open cell foams consisting of regular cells [3][21][22].Periodic open cellular structures were also studied experimentally: [23] investigated the effects of porosity and cell orientation on pressure drop. Regular structures are easier to handle because they require only two independent parameters (for example the characteristic pore dimension and its ratio to the strut diameter) and mathematical expressions allow obtaining all the other geometrical

properties [1]. The Kelvin cell has often been used as a typical elementary cell. A flow resistance comparison between Kelvin cells and foams has been performed by [24]. The flow pattern inside real and ideal foams at various Reynolds numbers has been investigated [25][26]. It has been demonstrated that regular open cells perform better than randomized foams [2]. In fact they always show a better trade off between mass transfer and pressure drop in respect to the equivalent real foams. So, regular cell lattices should be not seen only as a geometrical model, but as catalytic structures that outperform foams.

In the last years, advances in AM techniques have provided new possibilities for manufacturing [27][28][29]. Latest improvements have even allowed the direct manufacturing of ceramic lattices [30][31][32]. AM comprises several processing techniques where parts are fabricated by physical or chemical consolidation layer by layer, starting from a CAD file. A core concept, intrinsic in these AM techniques is the rapid and seamless transition between a computer model and the physical realization thereof [33].The revolution consists in the new approach of components' design by function and no longer by manufacturability [32]. Considering catalyst applications specifically, design is performed through an intensive campaign of numerical simulations, while AM stereolithography proved to be the most suitable process, allowing the manufacturing of extremely thin and complex structures with reduced flaw size [34]. The shape of conventional catalysts is determined to a large extent by the manufacturing methods, instead, the AM techniques have introduced a significant flexibility and a higher freedom in design. Big efforts have been spent in using additive fabrication tools for structured monoliths for improving mass and heat transfer characteristics with a higher geometric surface area [29]. In [35], with the support of CFD computations, robocasting is performed to create a ceramic face-centered-cubic structure with high surface to volume ratio able to convert approximately six times more methane than extruded monoliths. Robocasting is also used to fabricate Ti-alloy and stainless steel monoliths with well-controlled contact times [36]. 3D printing has also enabled to fabricate complex ceramic supports for use in packed beds [37], or reaction vessels and microreactors with integrated catalysts [38]. In all cases AM has led to improved performances through more complex structures, difficult to be produced by extrusion.

Thus, AM closes the gap between theory and experiment, by enabling accurate fabrication of a great variety of geometries, optimized through computational fluid dynamics and evaluated through experiments [29].

The present study adopts this new combined approach for the design of an open cell polyhedral lattice catalyst substrate for automotive applications. It identifies the optimal open cell polyhedral catalyst lattice in terms of shape and dimensions through detailed numerical simulations. The performance of the open cell lattice structures has been evaluated by the mass transfer coefficient, by the pressure loss per unit of length and by the dimensionless performance index I [3].

Based on simulations results, the polyhedral ceramic substrates have been manufactured with stereolithography, coated in house and then tested in a gas reactor. $C_3H_6$ oxidation has been measured at different gas hourly space velocities (ghsvs) as well as light-off behaviour. The integral approach that combines numerical simulations, AM realization, and experimental testing, is, to our knowledge so far, applied here for the first time for developing polyhedral lattice substrates as automotive catalyst supports.

## 2. SIMULATION METHODOLOGY

### 2.1 Numerical Approach

3D CFD simulations with the freely available software OpenFOAM have been conducted to define the optimal polyhedral lattice substrate geometry. The model adopted has already been validated and described in [1][12]. Different configurations have been constructed with the 3D CAD softwares Salome and Netfabb. No transient conditions have been considered and the catalyst is assumed to have reached steady state. The catalyst is studied in the mass transfer limited regime with infinite fast chemistry. This condition was imposed with a temperature of 700 K at inlet, clearly higher than light off. The goal is to compare several substrate configuration performances with an acceptable computational effort. A single region model has been adopted: the mesh represents the flow region and the boundaries are the inlet, the outlet and the catalyst surface. Based on the analysis from Lucci et al. [1], no conjugate heat transfer has been implemented and the heat exchange between flow and solid has been modelled by imposing a constant T=750K at the catalyst surface. Preliminary simulations [1] have shown a difference between the maximum and the minimum temperatures in the solid matrix of less than 3 degrees. Thus, since the inclusion of the conjugate heat transfer greatly increases the computational costs, we decided to neglect it. The hydrocarbon chosen for the simulations is methane $CH_4$. Homogeneous reactions are

neglected, while heterogeneous reactions are treated as boundary conditions at the catalyst surface, imposing a null concentration for the oxidized specie $CH_4$ and a gradient of the other species corrected on the basis of the reaction stoichiometry:

$$\frac{\partial X_i}{\partial n} = \alpha_i \frac{MM_i}{MM_{CH4}} \frac{\partial X_{CH4}}{\partial n} \qquad (1)$$

Where $\alpha_i$ is the stoichiometric coefficient of specie i ($\alpha_{CH4}$=1). In order to guarantee the mass balance, an inert element, $N_2$, has been chosen. Constant transport properties of chemical species have been specified while the thermal model was based on constant enthalpy. Species are assumed to have Schmidt number equal to 1, which means that diffusivity equals the kinematic viscosity. For saving computational time, taking advantage from the regularity of the open cell substrate, only a fraction of the overall catalyst volume has been studied (see Fig. 1). In both the two cross flow directions cyclic boundary conditions are applied [12]. No washcoat was modelled. The mesh is built automatically with a background mesh and the application "snappyHexMesh" of OpenFOAM (see Fig. 2). The mesh has been extended both before and after the catalyst position in order to have uniform flow conditions at the catalyst inlet and to avoid boundary conditions problems at outlet. At inlet, the conditions imposed are: fixed temperature, velocity and species concentrations. At outlet, the conditions are: ambient pressure and "zero gradient" for temperature, velocity and species concentrations at outlet**.** A grid of around 5 million hexahedral elements allows obtaining a grid independent solution..

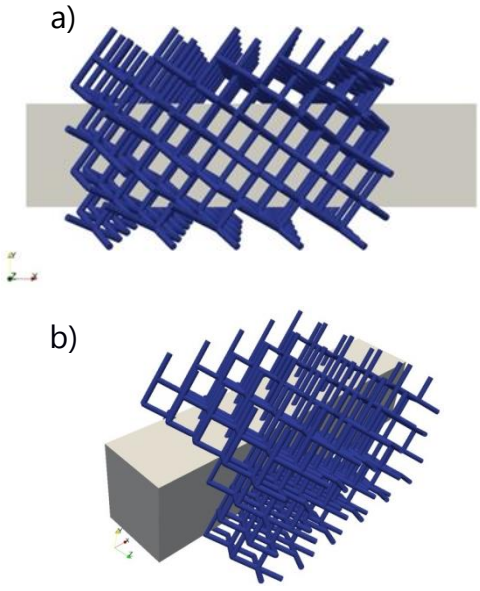


Fig. 1 Example of flow domain studied for Cubic45 structure (see Section 2.2) in two different perspectives (a) and b)).

The grid independence analysis was carried out by modifying the background mesh dimensions (reference, coarser, finer).The efficiency of each structure has been extracted for different inflow velocities (1, 5, 10 and 15 m/s) and expressed in terms of mass transfer coefficient K, pressure loss per unit of length and performance index I

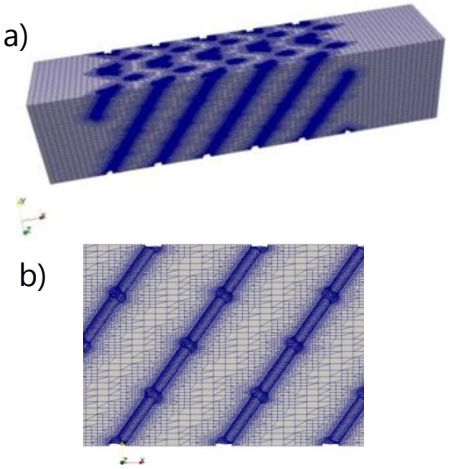


Fig. 2 Entire mesh (a)) and its detail (b)). The mesh is obtained with a background mesh and the application "snappyHexMesh" in OpenFOAM.

**2.2 Elementary Cells**

Three different elementary cell geometries have been chosen as a basis for the simulations, Cubic, Kelvin, and Octet (Fig. 3). The cubic elementary cell is introduced in the simulations with two different orientations, parallel and rotated by 45° so that one spatial diagonal of the cube is aligned to the main gas flow. Throughout this paper these elementary cells are referred to as Cubic, Cubic45, Kelvin and Octet. A systematic geometrical investigation has been performed. The main parameters are the strut diameter ($d_s$), the strut length ($L_s$), the cell length ($L_c$), the porosity ($\varepsilon$) and the specific surface ($S_v$). Two of these parameters can be set independently leading to the determination of the remaining. Analytical expressions have been derived for the computation of $\varepsilon$ and $S_v$ in function of $d_s$ and $L_s$ for the different cell geometries [39].

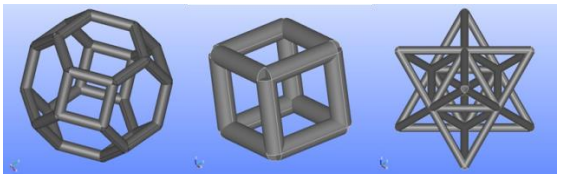

Fig. 3: Kelvin, Cubic and Octet used as elementary cells for simulating catalytic converter behaviour.

### 2.3 Volume Averaged Considerations

The procedure adopted to compute the mass transfer coefficients is explained in [1]. It should be reminded that the mass transfer coefficient, K, is directly related to the conversion η that can be achieved by a catalyst of certain dimensions (length L, cross section A, overall volume V, specific surface area $S_v$, and wetted surface area $S_w$), in a gas flow of a certain inlet velocity, $v_{in}$, as shown in Eq. (2).

$$K = \frac{-ln(1-\eta)}{S_w}\dot{Q}_{in} = \frac{-ln(1-\eta)}{S_v V}Av_{in} = \frac{-ln(1-\eta)}{S_v L}v_{in} \quad (2)$$

Higher mass transfer may be accompanied by higher flow-through resistance. For relating the two, the performance index I has been introduced [3] as in Eq. (3).

$$I = \frac{-ln(1-\eta)}{\Delta P}\rho {v_{in}}^2 = \frac{KS_v L\,\rho v_{in}}{\Delta P} \quad (3)$$

## 3. REALIZATION OF POLYHEDRAL OPEN CELL CATALYTIC CONVERTER SAMPLES

### 3.1 Additive Manufacturing

Substrate samples have been additive manufactured by stereolithography. Details concerning fabrication, microstructural and mechanical properties of the samples can be found in [32]. Based on initial simulation results, described in Section 5.1, two different Cubic45 polyhedral structures have been printed in cylindrical shapes of dimensions of 12mm in diameter and 20mm in length. Fig. 4 shows one of the AM Cubic45 3mm samples. The prepared samples differ in strut length of 3mm and 4mm respectively and thus in cell sizes, porosities and specific surfaces. Strut diameter, $d_s$, and strut length, $L_s$, have been measured on the realised samples and confirmed by SEM images (Fig. 5). The major geometrical characteristics of the realised samples are summarized in Table 1. For all AM substrates the material used has been $Al_2O_3$.

| Cell geometry | ε [-] | $d_s$ [mm] | $L_s$=$L_c$ [mm] | $S_v$ [$m^2/m^3$] |
|---|---|---|---|---|
| Cubic45 3mm | 0.90 | 0.6 | 3.0 | 630 |
| Cubic45 4mm | 0.95 | 0.6 | 4.0 | 353 |

Table 1: Geometrical characteristics of the realized substrate samples.

AM and material effects on porosity have not been considered. No material micro-porosity is taken into account since it is not active for the catalyst (it is covered by the washcoat). For the same reason, the surface corrugation and related porosity effect of the AM layers having some 30-50μm of diameter variation is neglected.

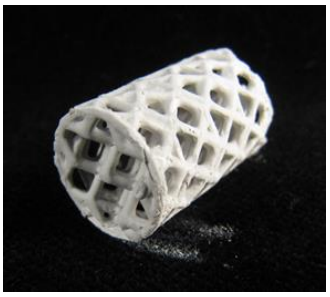

Fig. 4: Image of an AM lattice (material $Al_2O_3$) with Cubic45 elementary cells (gas entrance through the top circular cross section), after catalytic coating, as used in the model gas reactor.

The benchmark for the AM substrates is a conventional, extruded 400cpsi cordierite HCs. Samples had to be extracted from monoliths of larger dimensions. The goal was to have identical outer dimensions with the AM counterparts (i.e. 12mm diameter and 20mm length).The length of the samples showed variations for almost ±1.5mm due to the uncertainties of the extraction. Finishing of the HC pieces aimed at samples comprising identical channel number. A comparison of the geometrical data in Tables 1 and 2 underlines the substantial difference in specific surface areas; the HC has roughly 6 times higher specific surface area in respect to the AM Cubic45 4mm lattice.

| ε [-] | CPSI [-] | $D_c$ [mm] | $d_c$ [mm] | $r_c$ [mm] | $L_c/D_c$ [-] | $S_v$ [$m^2/m^3$] |
|---|---|---|---|---|---|---|
| 0.73 | 400 | 1.25 | 1.125 | 0.375 | 30 | 2480 |

Table 2: Geometrical properties of the conventional HC substrate.

### 3.2 Coating of the substrates

All substrates have been coated in house by dipping the samples. The identical solution, consisting of a γ-$Al_2O_3$-Pt suspension (also prepared in house), has been used for coating all substrates. The goal was to apply identical type and amount of coating and thus Pt amounts on all samples. This implies that, considering the different ε of open cell structures and HCs, with the latter that have larger surface, a thicker washcoat layer is present on the open cells with respect to HCs. Some variation among the individual samples is inevitable, especially given the different adhesion properties of the materials and geometries and has to be accounted for when discussing reactivity results.

The coating method applied was chosen based on [40][41][42], and variations were performed

for achieving better results in our laboratory. The procedure of coating through dipping consists in dissolving Tetraamineplatinum in water, then γ-$Al_20_3$ is added and the suspension is stirred for 24 hours. The goal is homogeneous Pt content, around 1.5 weight%. In a next step the water is dried and calcination follows at 500°C in the furnace. The resulting powder is milled in order to reduce the agglomerates. Subsequently, the powder is dissolved in water in order to obtain the slurry. pH value affects the quality of the coating [43], thus a pH adjusting additive is used to maintain the pH value around 10. The slurry is then ball-milled for 48h with $ZrO_2$ balls. Substrates are dipped in the slurry thereafter. Excess slurry is blown off. The last step consists in drying the coated substrates at 600°C. In Table 3 we summarize the average values for the characteristics of the coating on the substrates in question.

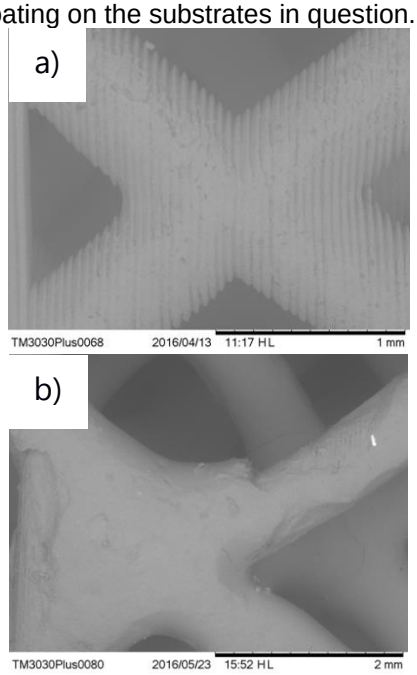


Fig. 5: SEM images: a) AM substrate with evident AM layers, b) AM substrate with washcoat. On the central strut clearly discernible is the coating thickness adding ¼ to the strut diameter (=150μm).

| Substrate | Cubic45 3mm | Cubic45 4mm | HC |
|---|---|---|---|
| Substrate mass [g] | 0.84 | 0.77 | 0.76 |
| Coating mass [%] | 35 | 34 | 38 |
| Spec. coating [g/lt] | 131 | 117 | 128 |
| Pt [mg] | 4.3 | 3.8 | 4.5 |
| Pt [g/lt] | 1.93 | 1.7 | 1.98 |
| Pt [g/ft$^3$] | 54 | 47 | 53 |
| Average coating thickness [μm] | 75 | 130 | 40 |

Table 3: Major characteristics of the coated substrates, average values of at least 4 samples.

Table 3 reveals a general similarity of the results of the coating procedure on all different substrates. The data are typical for coatings of state of art automotive catalysts. The thickness of the coating on the AM lattice catalysts is substantially higher than in the HC. Thus, in AM substrates, the inner part of the coating is certainly not reached by the gases in the reactions and thus is superfluous. A modified coating procedure is needed in order to arrive to coatings with less thickness on the AM substrates. The high coating thickness was confirmed by SEM images as shown in Fig. 5b.
Taking into account the resulting coated strut diameters, the geometrical characteristics of the samples are summarized in Table 4.

| Cell geometry | ε [-] | $d_s$ [mm] | $S_v$ [m$^2$/m$^3$] |
|---|---|---|---|
| Cubic45 3mm | 0.85 | 0.75 | 785 |
| Cubic45 4mm | 0.89 | 0.86 | 507 |

Table 4: Geometrical characteristics of the coated substrate samples.

## 4 EXPERIMENTAL SETUP

Catalytic activity of the different samples, both HC and AM polyhedral lattices, has been evaluated experimentally in a tube quartz reactor ($\varphi$=13mm) placed in a furnace (Fig. 6). The feeding gas mixture has been set by mass flow controllers to be 500ppm $C_3H_6$, 8% $O_2$ balanced with $N_2$. The temperature of the oven is imposed and the flow is partially preheated up to a chosen temperature. The temperature distributions have been measured by thermocouples, while the chemical conversions have been monitored by gas phase FTIR using a Nicolet 5700 spectrometer equipped with a gas cell. Experiments have been conducted either at constant flow rate and increasing oven temperature (temperature profile imposed is a ramp from 50°C to 600°C with a heating ramp of 10°Cmin$^{-1}$), in order to obtain the light-off curves, or at constant temperature but with increasing flow rate for understanding the impact of the flow velocity on reaction rates.

Fig. 6: Model Gas Reactor.

## 5 RESULTS AND DISCUSSION

### 5.1 Simulation results

#### 5.1.1 Elementary cell variation

In this section detailed simulation results are used for comparing the mass transfer and pressure drop characteristics of catalysts consisting of different elementary cells in the mass transfer limited regime. Comparisons involve cells with identical, high porosity (ε=0.95) and rather small strut diameter (considering manufacturing feasibility, $d_s$=0.5mm is imposed). Thus, the compared elementary cells have identical $S_v$ (400m$^2$/m$^3$) but different $L_c$. The detailed geometrical characteristics computed with analytical expressions are reported in Table 5. Table 2 shows the corresponding geometrical characteristics for the conventional HC substrate. In Fig. 7a displayed are the simulated mass transfer coefficients over the inflow gas velocity for the different elementary cells under consideration. The HC is also included for a comparison with the current standard catalyst substrate. Computation and results concerning mass transfer in HCs have been taken from previous papers [1][2][8].

| Cell geometry | ε [-] | $d_s$ [mm] | $L_s$ [mm] | $L_c$ [mm] | $S_v$ [m$^2$/m$^3$] |
|---|---|---|---|---|---|
| Kelvin | 0.95 | 0.5 | 2.04 | 5.77 | 400 |
| Cubic/Cubic45 | 0.95 | 0.5 | 3.43 | 3.43 | 400 |
| Octet | 0.95 | 0.5 | 5.77 | 8.17 | 400 |

Table 5: Geometrical properties of the AM structures with ε=0.95 and $d_s$=0.5mm.

Fig. 7a evidences that, due to the increasing flow-wall interaction, mass transfer improves with increasing gas velocity for each of the examined cell geometries. Mass transfer in the HC, in contrast, has a significantly weaker dependency on velocity (mainly due to the laminar flow inside the channels). All open cell polyhedral structures have clearly higher mass transfer coefficients, K, than the HC. Specifically, Cubic45 has the highest, while Kelvin and Octet have almost identical, and Cubic the lowest mass transfer coefficient. These better mass transfer properties of open cell substrates are related to their more intricate geometries that increase the contact probability of the species with the solid surfaces and the mixing. The flow around the struts results in boundary layers and separation regions which are constantly evolving, leading to enhanced transport.

Taking into account the two polyhedral structures based on a cubic elementary cell, first, the orientation of the structure with respect to the flow can lead to gain a factor of 2.3 at 10m/s (comparison between Cubic and Cubic45). Second, to make a quantitative comparison, the mass transfer coefficient of the Cubic45 is 4 times higher than the corresponding one of the HC at 10m/s. According to Eq. (2), for reaching a certain conversion, η, the K coefficient is inversely proportional to the necessary wetted surface $S_w$ (at a fixed gas flow rate $Q_{in}$). This means that, at steady state and in similar conditions, Cubic45 (with ε=0.95, $d_s$=0.5mm) can achieve the same conversion with only 1/4 of the HC wetted surface. Should washcoat properties and thicknesses be similar for each catalytic support, a reduction in necessary wetted surface area corresponds to an equivalent reduction in required noble metals. However, Cubic45 has 1/6 lower specific surface area with respect to HC (see $S_v$ in Tables 2 and 5). By rearranging the Eq. (2) in Eq. (4), it is evident that, in similar conditions, Cubic45 will achieve the same conversion rate with 3/2 of the volume (larger catalyst).

$$KS_v = \frac{-ln(1-\eta)}{V} A v_{in} = \frac{-ln(1-\eta)}{L} v_{in} \quad (4)$$

These considerations are valid in the mass transfer limited regime. Instead, during cold start, where the time scale of chemical reactions is crucial, the better heat transfer characteristics of the polyhedral substrates (analogous to the higher mass transfer properties) in combination with the higher porosity (lower mass) may be able to overcome the deficiency of the lower precious metals. In a former work [7] comparable cold start emission characteristics of HCs and Kelvin cell structures have been estimated, although the latter have substantially less precious metal amount.

For each open cell geometry, in the range examined, the pressure loss increases exponentially with increasing velocity, while HCs are characterized by a linear dependence of pressure loss on velocity. Open cell substrates with high porosity like 0.95 show a lower pressure loss per unit of length with respect to HCs (Fig. 7b). This is not valid with open cells with lower ε, as can be seen in Section 5.1.2. Of interest is the ratio as expressed by the performance index, I, introduced by Eq. (3) and shown in Fig. 7c. The performance index, however, is only weakly dependent on velocity for all geometries examined. Certainly, at low velocities, the performance is higher, and thus the imperative is always to operate at the lowest possible velocities, implying an increase of the inlet flow cross section area. On the other hand, for

all velocities, the open cell structures are characterized by higher performance indexes in respect to the HC. The Cubic45 (with ε=0.95, $d_s$=0.5mm) outperforms all other structures. Thus it is the most promising structure for a catalyst substrate.

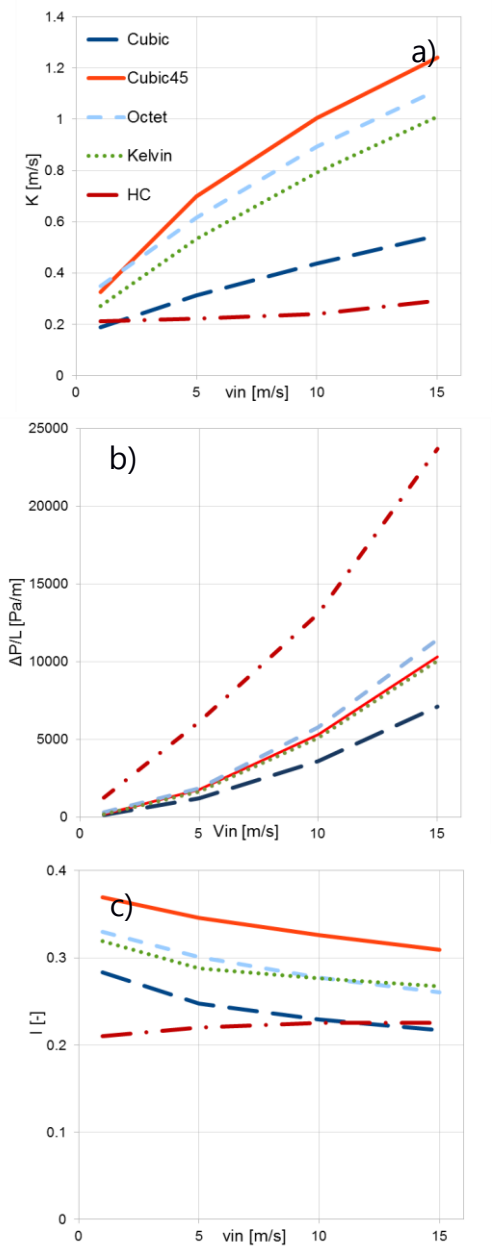


Fig. 7: Comparison of different AM elementary cell configurations (all with ε=0.95, $d_s$=0.5mm) and the HC in terms of mass transfer coefficients, K (a), pressure drop per unit of length (b), and performance indexes, I (c).

The parameter K is best suited for comparing different substrates geometries due to its inverse proportion with $S_w$. A non dimensional comparison between the different substrates described in Table 5 and HC is shown in Fig. 8. In Fig. 8 the Sherwood number (Sh) computed from the simulations is plotted in function of Re. The Cubic45 elementary cell has the highest Sh number, while the Sh number associated with the Octet elementary cell are lower. The Cubic elementary cell results to the lowest Sh number. The Computation and results concerning HCs have been taken from previous papers [1][2][8]. Correlations concerning the asymptotic behaviour of HC at low Re are confirmed [44]. Note that for Sh and Re numbers of AM structures, for the characteristic length, we use $d_s$. HC correlations use $D_c$. Thus a direct comparison is not straightforward. The Sh numbers of HC, however, are higher in the low velocity domain in respect to the Sh number of the AM substrates. At higher velocity, the tendency is reverse.

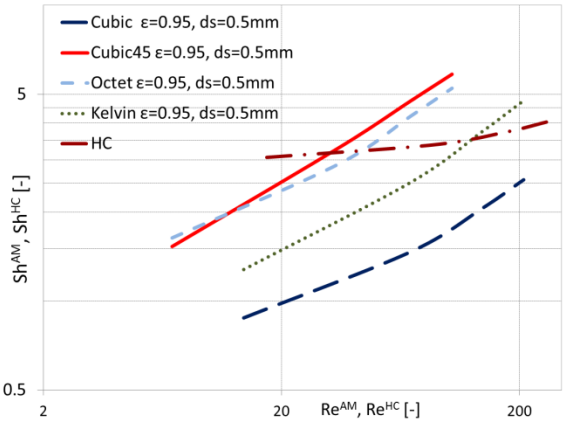


Fig. 8: Sherwood number versus Reynolds number for different AM elementary cell configurations (all with ε=0.95, $d_s$=0.5mm) and the HC. The characteristic length for Sh and Re of the AM elementary cell configurations is $d_s$, while for HC is $D_c$.

### 5.1.2 Porosity variation

The very high porosity used in the comparisons of the former section showed clear performance index advantages but led to relatively high catalyst dimensions (required to obtain a certain conversion) because of the low specific surface area. The latter can be increased by decreasing the porosity. In this section CFD results of Cubic45 and Kelvin elementary cell geometries are compared (the strut diameter is constant and equal to the one chosen in the former section, $d_s$=0.5mm) at different porosities (ε =[0.8, 0.85, 0.9, 0.95]). The detailed geometrical dimensions of the catalysts in comparison are reported in Table 6. The lower porosities result in more dense structures with higher specific surface areas $S_v$.

In Fig. 9a the mass transfer coefficients over the inflow velocity are plotted. Cubic45 is chosen because it represents the most promising elementary cell geometry according to Figs. 7a and 7c. The Kelvin cell is chosen because it does not lack significantly in performances and it is already an item of different studies as a

good idealization of real foams [1][2][7][20][21][24][25].
It is clear that the K coefficient decreases with increasing porosity. For instance, considering Cubic45 at 10m/s, the K coefficient increases by a factor of 1.28 with decreasing porosity from ε=0.95 to ε=0.8. This implies that, in similar conditions, Cubic45 with lower porosity can achieve the same conversion rate with only 0.78 (1/1.28) of the $S_w$ and noble metals required by the same geometry at higher porosity. Cubic45 with ε=0.8 has 4 times the specific surface of Cubic45 with ε=0.95, as can be seen in Table 6. It is evident that, in similar conditions, Cubic45 with ε=0.8 can achieve the same conversion rate with 5.1 (=1.28*4) times less volume than Cubic45 with ε=0.95. Considering constant inlet cross section, this means 5.1 times reduced catalyst length. Comparing the two different open cell geometries, Cubic45 confirms its superiority in respect to Kelvin at each porosity.

| Cell type | ε [-] | $d_s$ [mm] | $L_s$ [mm] | $L_c$ [mm] | $S_v$ [$m^2/m^3$] |
|---|---|---|---|---|---|
| Kelvin | 0.8 | 0.5 | 1.02 | 2.88 | 1600 |
| Cubic45 | 0.8 | 0.5 | 1.72 | 1.72 | 1600 |
| Kelvin | 0.85 | 0.5 | 1.18 | 3.33 | 1200 |
| Cubic45 | 0.85 | 0.5 | 1.98 | 1.98 | 1200 |
| Kelvin | 0.9 | 0.5 | 1.44 | 4.08 | 800 |
| Cubic45 | 0.9 | 0.5 | 2.43 | 2.43 | 800 |
| Kelvin | 0.95 | 0.5 | 2.04 | 5.77 | 400 |
| Cubic45 | 0.95 | 0.5 | 3.43 | 3.43 | 400 |

Table 6: Geometrical properties of AM structures based on the Kelvin and Cubic elementary cell with $d_s$=0.5mm

The implications with AM structures having lower porosity in respect to the conventional HCs are of particular interest. Based on the analysis above, it is clear that the Cubic45 cell with the low porosity, ε =0.8, can achieve the conversion of a HC catalyst with significantly lower wetted surface (5 times lower at gas velocity of 10m/s) and thus also with significantly lower precious metals (approx. also 5 times lower at 10m/s) as well as with a lower overall volume (approx. 3 times lower).
On the other hand, though, the pressure drop is expected to increase with decreasing porosity. The performance index, I, for the same set of cell geometries is reported in Fig. 9b in function of the inflow velocity. It is clear that porosity must be maximized in order to obtain the highest I values. For instance, the I performance index for Cubic45 at 10m/s increases 1.5 times from ε=0.8 to ε=0.95. The figure also confirms the outperformance of Cubic45 with respect to Kelvin at every porosity. Thus, on the whole, Cubic45 with maximum porosity is the most promising structure for a catalyst substrate. Comparing Figs. 7c and 9b, it is evident that the performance index for the Cubic45 with a porosity of ε=0.8 lies slightly below the corresponding one of the HC. As long as we are interested in structures that allow to outperform with respect to the benchmark of HC, examining lower porosities for the open cell structures was not considered of importance.

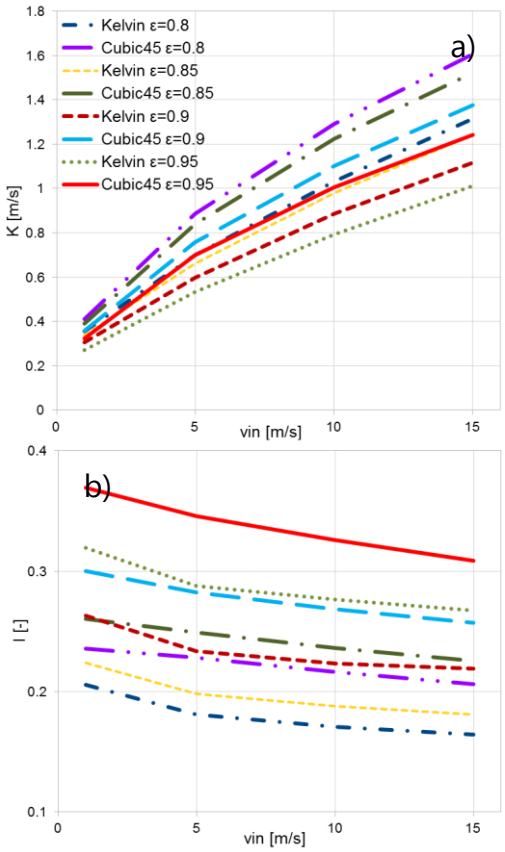


Fig. 9: Comparison of Kelvin and Cubic45 elementary cell configurations (all with $d_s$=0.5mm) in terms of mass transfer coefficients, K (a), and performance indexes, I (b).

### 5.1.3 Strut diameter variation

Manufacturing of polyhedral catalyst substrates with SLA directly, using ceramic materials, as cordierite, is possible, as shown in this study. Upscaling the method for real vehicle size catalysts and for large numbers is, at least for the moment, very time consuming. A feasible way to overcome this problem maybe the use of hybrid techniques. Currently, an option to produce ceramic substrates therefore could be the additive manufacturing of an organic scaf-

fold which then will be used as a basis for the well-established replica method in order to arrive to ceramic substrates. Such a method will lead to larger strut diameters in respect to the smallest achievable through direct SLA with the ceramic material. Therefore, a series of simulations has been performed in order to analyze the effects of larger strut diameters. The strut diameter affects the porosity as well as the specific surface of a substrate. The porosity, ε, is a function of the ratio $d_s/L_c$, while $S_v$ is a function of the ratio $d_s/L_c$ as well as of $L_c$. Should double strut diameters (1mm instead of the 0.5mm assumed up to now) be the result of the manufacturing process, then double strut and cell lengths are required for keeping constant the porosity. This, in turn, reduces the specific surface to the half. A series of detailed simulations has been performed for analysing the mass transfer and pressure drop characteristics of structures consisting of Cubic45 elementary cells with two different strut diameters (0.5mm and 1mm) at different porosities. Table 7 summarizes the geometrical characteristics of the compared substrates.

| Cell geometry | ε [-] | $d_s$ [mm] | $L_s=L_c$ [mm] | $S_v$ [$m^2/m^3$] |
|---|---|---|---|---|
| Cubic45 | 0.8 | 0.5 | 1.72 | 1600 |
| Cubic45 | 0.8 | 1 | 3.43 | 800 |
| Cubic45 | 0.85 | 0.5 | 1.98 | 1200 |
| Cubic45 | 0.85 | 1 | 3.96 | 600 |
| Cubic45 | 0.9 | 0.5 | 2.43 | 800 |
| Cubic45 | 0.9 | 1 | 4.85 | 400 |
| Cubic45 | 0.95 | 0.5 | 3.43 | 400 |
| Cubic45 | 0.95 | 1 | 6.86 | 200 |

Table 7: Geometrical properties of AM structures based on the Cubic45 elementary cell.

The mass transfer coefficients of catalysts consisting of Cubic45 elementary cells and different geometrical characteristics are shown in Fig. 10a. Clearly, with increasing strut diameter, the mass transfer coefficients decrease, for all examined porosities. For instance, at 10m/s and ε=0.85, the K coefficient with $d_s$=0.5mm is 1.47 times the K with $d_s$=1mm. In addition, decreasing porosity leads to higher mass transfer coefficients, a trend already seen in Fig. 9a and here confirmed for different $d_s$.
For the same set of configurations, the performance index I is plotted in Fig. 10b. The porosity affects I more strongly than the strut diameter. Thus, the highest performance indices are associated with the substrates having the highest porosities. The strut diameter has clearly a smaller influence.

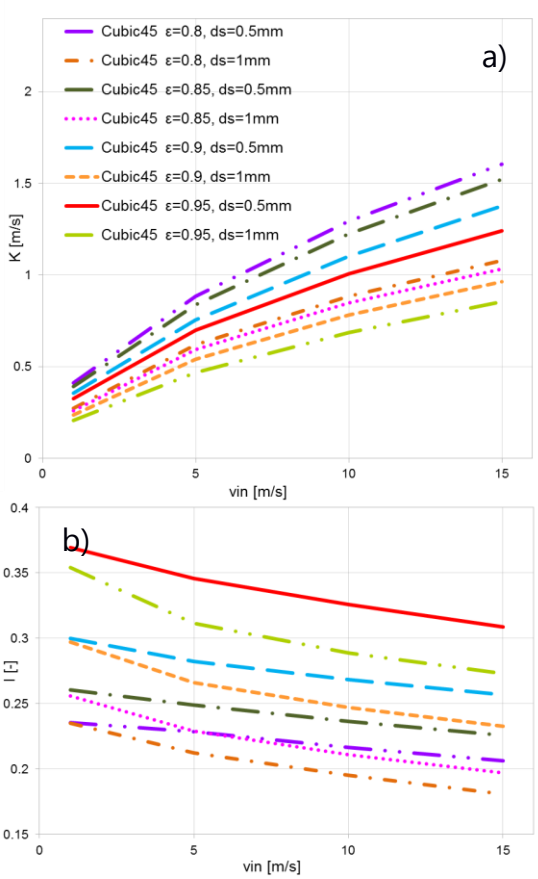


Fig. 10: Comparison of mass transfer coefficients, K, of Cubic45 elementary cell configurations and different geometrical characteristics in terms of mass transfer coefficients, K (a), and performance indexes, I (b).

Table 8 summarizes the characteristics of selected polyhedral catalysts in relation to the ones of the HC benchmark for achieving an identical conversion at gas flow velocity $v_{in}$ of 10m/s. The high porosity and high strut diameter case (ε=0.95 and $d_s$=1.0mm) results in 2.8 times higher mass transfer in respect to the HC, requiring 2.8 times less wetted surface (and as long as reactions are mass transfer limited, less precious metals) for achieving identical conversion. This substrate, however, has 12 times less specific surface area. Thus, for achieving the same conversion, a 4.3 times higher catalyst volume is required. This additional length leads to pressure drop increase. This is though not detrimental since the performance index is around 1.4 times the conventional HC. In contrast, the substrate with lower porosity and the lowest strut diameter (ε=0.85 and $d_s$=0.5 mm) can reach the identical conversion with even smaller volume in re-

spect to the HC (0.4 times). The high reactivity resulting from the higher strut density and flow-solid interactions results in higher pressure drop. Thus, the performance index advantage in respect to the HC is lower with respect to Cubi45 with higher porosity.

| Cubic45/HC | K (~1/$S_w$) | $S_v$ | V | I |
|---|---|---|---|---|
| ε=0.95, $d_s$=1mm | 2.8 | 1/12 | 4.3 | 1.4 |
| ε=0.85, $d_s$=1mm | 3.5 | 1/4 | 1.2 | 1.0 |
| ε=0.95, $d_s$=0.5mm | 4.1 | 1/6 | 1.5 | 1.6 |
| ε=0.85, $d_s$=0.5mm | 5.1 | 1/2 | 0.4 | 1.2 |

Table 8: Characteristic mass transfer, catalyst dimensions and performance index relations of selected AM polyhedral lattice catalysts in respect to the HC benchmark for identical pollutant conversion and $v_{in}$=10m/s.

### 5.1.4 Effects of washcoat on geometry

The effects of washcoat on the AM samples described in Section 3.1 are here considered. The presence of washcoat on substrates introduces an extra diffusion resistance and affects the geometrical parameters ($d_s$ increases, ε decreases). In this section, only the geometrical variations are discussed in terms of mass transfer coefficient K and performance index I (Fig. 11). Washcoat diffusion effects have been studied in [45]. The original dimensions are in Table 1, while the resulting ones are in Table 4. The two substrates have a similar ε variation, while $d_s$ increases more on Cubic45 with $d_s$=4mm. The results are obtained through simulations of substrates with identical dimensions of the AM samples.

Increasing ε decreases K (see Fig. 9), and increasing $d_s$ (see Fig. 10) decreases K, thus the two effects due to washcoat level off (in terms of K). This is evident in Fig. 8a for Cubic45 with $d_s$=3mm. Even Cubic45 with $d_s$=4mm does not have a dramatic decrease of K. More relevant variations are in Fig. 8b. For instance, the I index of Cubic45 with $d_s$=3mm decreases of a factor of 1.18 at vel=10m/s due to washcoat, while of Cubic45 with $d_s$=4mm decreases of a factor of 1.26.

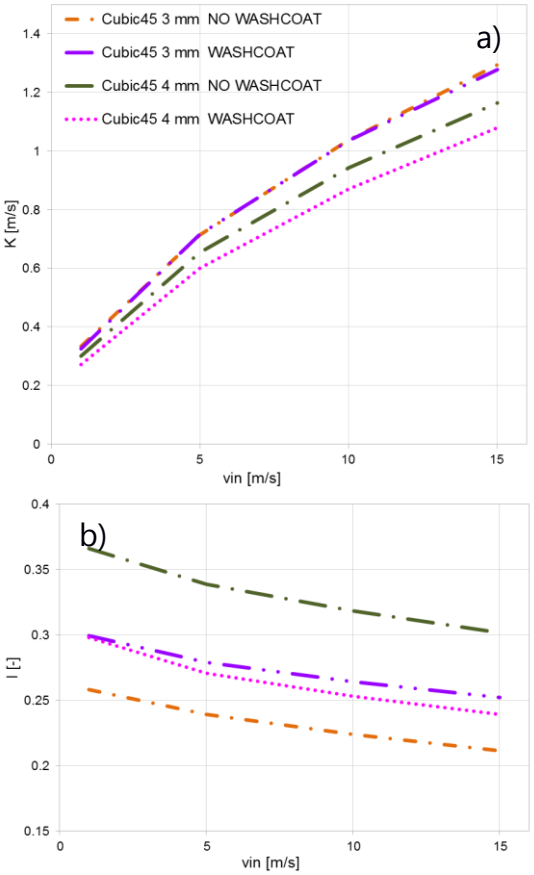


Fig. 11: Study of the geometrical effects of washcoat on AM substrates in terms of mass transfer coefficients, K (a), and performance indexes, I (b).

### 5.2 Experimental Model Gas Reactor Results

In the model gas reactor the oxidation of $C_3H_6$ has been quantified for a number of different manufactured and coated AM polyhedral substrates and their corresponding HC counterparts. Based on this conversion the corresponding mass transfer coefficients K have been computed assuming mass transfer limitation (assumption justified at T>400°C).

AM polyhedral substrates and HCs have been coated by the identical slurries always in one batch. However, two different variabilities have to be taken into account: 1) the honeycomb samples extracted from larger pieces had, as already discussed under section 3.1, some ±8% variability in length; 2) AM samples had well defined dimensions but some ±12% variability in the coating mass that was permanently attached to the samples. Therefore, plotted are the mass transfer coefficients over the Pt amount of each sample (Fig.12). From Fig. 12 it is evident that the resulting mass transfer coefficients are not dependent on the Pt amount (at least for the AM polyhedral substrates). It is also clear, that the AM polyhedral cells have mass transfer coefficients being more than

double as high as the HC. This is good confirmation of the simulation results (Fig. 7) which predict more than double mass transfer of the AM structures in respect to the HCs in this velocity domain.
The available model gas reactor did not allow measurements with higher gas velocities, i.e. higher ghsvs. At higher gas velocities the advantages of the AM substrates are expected to be substantially higher. The gas velocities, $v_{in}$, corresponding to the ghsvs tested, are 0.33m/s and 0.66m/s in Figs. 12a and 12b respectively.

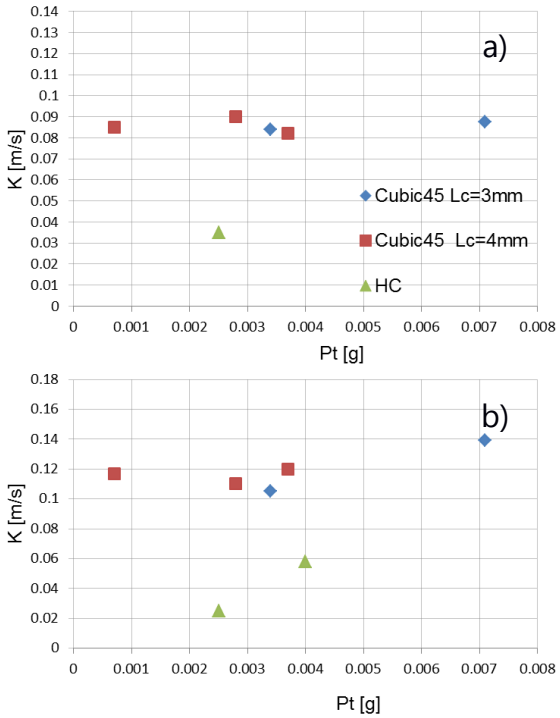


Fig. 12: Mass transfer coefficients computed from the conversion measurements in the model gas reactor for two different ghsvs ( a) 60000 $h^{-1}$,$v_{in}$=0.33m/s, and b) 120000 $h^{-1}$, $v_{in}$=0.66m/s)

These velocities are among the lowest used in the simulations (compare Fig. 7) and correspond to the lowest gas velocities in automotive catalyst applications. The mass transfer coefficients predicted by the simulations have been 4 times higher for the AM as well as for HC structures. Most probably this is a consequence of the restricted reactor and probe dimensions (comprising only 3-4 cells for the AM substrates and 9 channels for the HC) where boundary effects are over-pronounced as well as of the washcoat diffusion resistance, neglected in the simulations, but expected to be significant especially in the AM structures. Previous work has shown that the washcoat diffusion resistance has increasing impact when the substrate mass transfer resistance decreases (as is the case with the AM substrates) [39].
The results in terms of the achieved $C_3H_6$ conversion are displayed in Fig. 13. The conversion reached by the additive manufactured substrates seems to be independent of their Pt loading, as expected in the mass transfer limited domain.

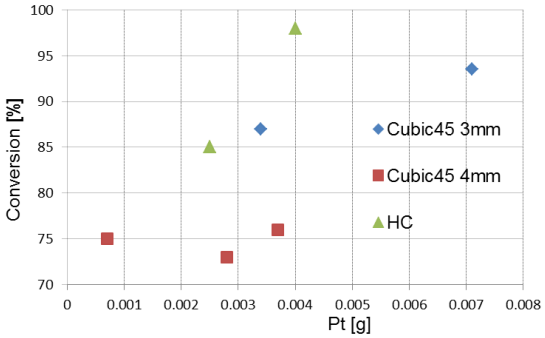


Fig. 13: $C_3H_6$ oxidation performance of the different substrates measured in the model gas reactor.

The achieved conversion by the HCs showed a higher sensitivity to the Pt amount due to the variation in the length of the extracted HC pieces. On the other hand, the conversions achieved by the HCs and the Cube45 3mm are very similar, while the conversions achieved by the Cube45 4mm are clearly lower. It has, though, to be kept in mind, that the Cube45 3mm and the Cube45 4mm achieved these conversions with respectively 4 and 7 times smaller surface area.
The conversion characteristics of three of these substrates at different temperatures are shown in the light-off curves in Fig. 14. The conversion at low temperatures is very similar for all. Small differences in the conversion slope after 130°C are not clearly discernible and are better visualized in Fig. 15. At higher temperatures, approaching the mass transfer limited domain, the lower surface area of the AM substrates is the limiting factor. Above 300°C, however, the differences among the two HCs and the Cube45 3mm substrate are very small.
In Fig. 15 displayed are the evaluated light-off temperatures (temperature for reaching 50% conversion) of all substrates in the model gas reactor in relation to Pt contents. It is clear to be seen that the light-off temperatures decrease with increasing Pt content. [39] have shown that at lower temperatures the slow chemical kinetics result in shifting the reaction area in deeper washcoat layers, thus more of the washcoat and more of the precious metals can be utilized. It is also clear that the Cubic45 3mm substrates behave exactly as the HCs although they have 4 times lower surface area, evidencing the far better heat transfer charac-

teristics. In addition, the Cubic45 4mm substrates lead to 20°C lower light-off temperatures (in spite the 7 times lower surface area). This has to be a consequence of the better heat transfer characteristics as well as of the lower mass of these substrates.

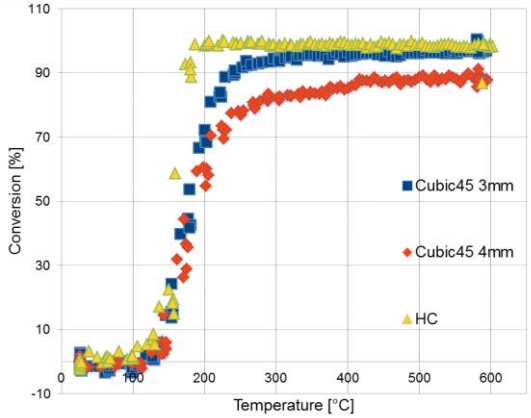


Fig 14: Light-off curves of four substrates at ghsv=60'000[$h^{-1}$]

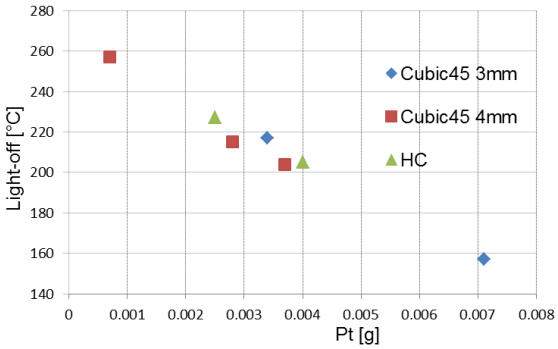


Fig. 15: Measured light-off temperatures of all examined substrates at ghsv=120'000[$h^{-1}$].

### 5.3 Characteristics of the Sherwood Number

A proposed way to analyse the external flow around objects is based on the selection of a characteristic length [46]. Several lengths have been proposed in the literature, posing difficulties for adequate comparisons for the flow through foams or packed beads. In [47] a comprehensive list of the used characteristic lengths has been presented together with the impact of the choice in the mass transfer laws. The choice of the characteristic length, in addition, has a strong impact in the definition of Re-number regimes characteristic for laminar, transition and turbulent flow patterns. In the present work the strut diameter $d_s$ was chosen as the characteristic length scale for the polyhedral lattices presented. Fig. 16 shows the dimensionless mass transfer coefficient, the Sherwood number, plotted over the Reynolds number, for the cases examined in Fig. 10. Fig. 16 clearly shows that the Sherwood number is almost independent of the strut diameter. This is a confirmation that the strut diameter may be an appropriate choice for the characteristic length. The question of the characteristic length can only be exhaustively answered by studying the flow patterns in detail, but this is beyond the scope of the present work.

Furthermore, in Fig. 16 an almost linear relationship between ln(Sh) and ln(Re) is evident. The slope is approx. 0.5 and thus the associated Sherwood law has to be an expression according to [47]:

$$Sh = C\, Re^{0.5} Sc^{\frac{1}{3}} \quad (5)$$

[3] proposed an exponent of 0.43 for the metallic foams examined. When dealing with flows across a bundle of tubes, [46] proposed an exponent of 0.4 for the laminar flow and 0.8 for the turbulent regime. Thus, the exponent proposed here shows that the regime $3<Re_{ds}<80$ dealt with in the present work is somewhere in the early transition regime. In addition, in Fig 16 there is a clear reciprocal dependency of the Sh on the porosity. So the expression in equation (5) has to be augmented in order to take this into account.

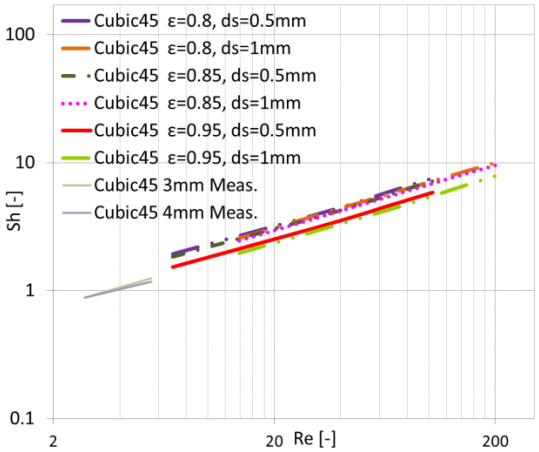


Fig. 16: Simulation and Experimental Sherwood numbers versus Reynolds numbers for Cubic45 substrates with different ε and $d_s$ (characteristic length for Sh and Re).

The dimensionless analysis allows a comparison between simulation and measurement results. In fact, the differences between simulations and measurements are such that other direct comparisons are less reasonable. The gas velocity domain simulated is substantially wider. The hydrocarbon assumed in simulations was methane while the hydrocarbon in the experiments was propane, the former having almost a double as high diffusion coefficient in respect to the latter. Thus, measured results of 3D Cubic45 samples were added.

The measured mass transfer values are lower than the values coming from simulations. This is most probably due to the very limited dimen-

sions available (the outer diameter of 12 mm comprises around 3-4 cells), as well as to the diffusion resistance through the washcoat (not considered in the simulations).

## 6. Conclusions

In this study, a comprehensive investigation of the properties of Additive Manufactured (AM) open cell polyhedral lattices has been performed with detailed numerical simulations, by systematic variation of the geometrical characteristics. The performance of the open cell structures was evaluated by the mass transfer coefficient, by the pressure loss per unit of length and by the dimensionless performance index I. Based on the simulation results, samples have been manufactured by stereolithography and coated with $Pt/Al_2O_3$. The reactivity of the samples has been assessed in a model gas reactor.

Simulations and experiments agree that mass transfer in flows through Additive Manufactured (AM) polyhedral structures increases substantially with increasing gas velocity and is several times higher in respect to the mass transfer through conventional HCs. Thus AM polyhedral structures require proportionally less gas wetted surface and accordingly less precious metals for achieving a target pollutant conversion (at high gas temperatures, where chemical reactions are mass transfer limited). For all AM structures examined, the following results can be summarized:

- Mass transfer increases with decreasing porosity.
- Pressure drop increases with decreasing porosity.
- Lower porosities had always the lower performance index.
- Lower porosities involve not only higher mass transfer, but also higher specific surface areas, thus requiring smaller overall catalyst volumes for a targeted conversion.
- Increasing strut diameters results in deterioration of the mass transfer, pressure drop, performance index and specific surface area.
- Among the examined elementary cell configurations, the Cubic45 cells exposed the best conversion to pressure loss ratio.
- At gas velocities of 10m/s, simulations show that Cubic45 cells with high porosity ($\varepsilon$=0.95) have 4 times higher mass transfer in respect to a standard HC. For achieving a target conversion this implies a fourth of the wetted surface and also a fourth of the precious metals, with about the half of the pressure drop. On the other hand the overall volume of the Cubic45 AM structure has to be 1.5 times higher than the HC, given the 6 times lower specific surface area.

The dimensionless mass transfer, as expressed by the Sherwood number (Sh) proved to be independent from the strut diameter, providing, at least partly, a justification for its selection as a characteristic length. Furthermore

- a linear dependency of the logarithm of the Sherwood from the logarithm of the Reynolds number has been determined.
- the slope of 0.5 of this dependency shows that the Re regime examined (3<re<80) lies in the early transition regime.
- a reciprocal dependency of the Sh number from the porosity was assessed.

Measured reactivities of first AM samples in a model gas reactor confirmed simulation results and revealed:

- Mass transfer of the AM structures is more than double as high as for HCs (in the lowest gas velocity domain) as also predicted by the simulations.
- Mass transfer and reactivities of the AM structures are independent on the Pt amount in the coating (at least in the variation domain of this study).

Achieving optimal results with the AM manufactured substrates requires careful matching of the coating, the chosen porosity and dimensions in order to reap a substantial potential for higher conversion, better light-off temperature with lower precious metals in the coating and lower flow through resistance.

## Acknowledgements

The authors gratefully acknowledge financial support from the Swiss National Science Foundation (SNF) for the project “Cases: Catalyst Substrates from Engineered Structures for state of the art powertrains: High pollutant conversion (including cold-start) with low precious metal requirements”, Project No 20PC21_161571/1, as well as from the Swiss federal Office for the Environment (FOEN) for the project “Development and manufacturing of an automotive catalyst concept for cold start low exhaust temperatures”, Project No UTF 522.14.15 IDM 2006.2423.485.

**Bibliography**


[1] F. Lucci, A. Della Torre, G. Montenegro, P. Dimopoulos Eggenschwiler, On the catalytic performance of open cell structures versus honeycombs, Chem. Eng. J. 264 (2015) 514–521. doi:10.1016/j.cej.2014.11.080.

[2] F. Lucci, A. Della Torre, G. Montenegro, R. Kaufmann, P. Dimopoulos Eggenschwiler, Comparison of geometrical, momentum and mass transfer characteristics of real foams to Kelvin cell lattices for catalyst applications, Int. J. Heat Mass Transf. 108 (2017) 341–350. doi:10.1016/j.ijheatmasstransfer.2016.11.073.

[3] L. Giani, G. Groppi, E. Tronconi, Mass-transfer characterization of metallic foams as supports for structured catalysts, Ind. Eng. Chem. Res. 44 (2005) 4993–5002. doi:10.1021/ie0490886.

[4] K. Pangarkar, T.J. Schildhauer, J.R. Van Ommen, J. Nijenhuis, F. Kapteijn, J.A. Moulijn, Structured packings for multiphase catalytic reactors, Ind. Eng. Chem. Res. 47 (10) (2008) 3720–3751.. doi:10.1021/ie800067r.

[5] G. Gaiser, J. Oesterle, J. Braun, P. Zacke, The Progressive Spin Inlet - Homogeneous Flow Distributions Under Stringent Conditions, SAE Technical Paper (2003-01-0840). doi:10.4271/2003-01-0840.

[6] K. Zygourakis, Transient operation of monolith catalytic converters: a two-dimensional reactor model and the effects of radially nonuniform flow distributions, Chem. Eng. Sci. 44 (1989) 2075–2086. doi:10.1016/0009-2509(89)85143-7.

[7] J. von Rickenbach, F. Lucci, P. Dimopoulos Eggenschwiler, D. Poulikakos, Pore scale modeling of cold-start emissions in foam based catalytic reactors, Chem. Eng. Sci. 138 (2015) 446–456. doi:10.1016/j.ces.2015.08.020.

[8] P. Dimopoulos Eggenschwiler, D.N. Tsinoglou, J. Seyfert, C. Bach, U. Vogt, M. Gorbar, Ceramic foam substrates for automotive catalyst applications: Fluid mechanic analysis, Exp. Fluids. 47 (2009) 209–222. doi:10.1007/s00348-009-0653-2.

[9] G.C. Koltsakis, D.K. Katsaounis, Z.C. Samaras, D. Naumann, S. Saberi, A. Böhm, I. Markomanolakis, Development of Metal Foam Based Aftertreatment System on a Diesel Passenger Car, (2008). doi:10.4271/2008-01-0619.

[10] M. V. Twigg, Progress and future challenges in controlling automotive exhaust gas emissions, Appl. Catal. B Environ. 70 (2007) 2–15. doi:10.1016/j.apcatb.2006.02.029.

[11] G. Montenegro, A. Della Torre, A. Onorati, G. Micci, G.M. Bianchi, S. Falfari, F. Brusiani, Design of Catalytic Devices by Means of Genetic Algorithm: Comparison Between Open-Cell Foam and Honeycomb Type Substrates, SAE International Journal of Engines, 9 (3) (2016), 1686-1695. doi:10.4271/2016-01-0965.

[12] F. Lucci, A. Della Torre, J. von Rickenbach, G. Montenegro, D. Poulikakos, P. Dimopoulos Eggenschwiler, Performance of randomized Kelvin cell structures as catalytic substrates: Mass-transfer based analysis, Chem. Eng. Sci. 112 (2014) 143–151. doi:10.1016/j.ces.2014.03.023.

[13] C. Hutter, A. Zenklusen, R. Lang, P. Rudolf von Rohr, Axial dispersion in metal foams and streamwise-periodic porous media, Chem. Eng. Sci. 66 (2011) 1132–1141. doi:10.1016/j.ces.2010.12.016.

[14] A. Della Torre, G. Montenegro, A. Onorati, G. Tabor, CFD characterization of pressure drop and heat transfer inside porous substrates, Energy Procedia. 81 (2015) 836–845. doi:10.1016/j.egypro.2015.12.093.

[15] A. Diani, K.K. Bodla, L. Rossetto, S. V. Garimella, Numerical investigation of pressure drop and heat transfer through reconstructed metal foams and comparison against experiments, Int. J. Heat Mass Transf. 88 (2015) 508–515. doi:10.1016/j.ijheatmasstransfer.2015.04.038.

[16] E. Bianchi, T. Heidig, C.G. Visconti, G. Groppi, H. Freund, E. Tronconi, An appraisal of the heat transfer properties of metallic open-cell foams for strongly exo-/endo-thermic catalytic processes in tubular reactors, Chem. Eng. J. 198–199 (2012) 512–528. doi:10.1016/j.cej.2012.05.045.

[17] W. Regulski, J. Szumbarski, Łaniewski-Wołłk, K. Gumowski, J. Skibiński, M. Wichrowski, T. Wejrzanowski, Pressure drop in flow across ceramic foams-A numerical and experimental study, Chem. Eng. Sci. 137 (2015) 320–337. doi:10.1016/j.ces.2015.06.043.

[18] G. Wehinger, H. Heitmann, M. Kraume, An artificial structure modeler for 3D CFD simulations of catalytic foams, Chem. Eng. J.284 (2016) 543-556. doi:10.1016/j.cej.2015.09.014.

[19] T. Wejrzanowski, J. Skibinski, J. Szumbarski, K.J. Kurzydłowski, Structure of foams modeled by Laguerre–Voronoi tessellations, Comp. Mater. Sci. 67 (2013) 216-221. doi:10.1016/j.commatsci.2012.08.046.

[20] M.Bracconi, M. Ambrosetti, M. Maestri, G. Groppi, E. Tronconi, A systematic procedure for the virtual reconstruction of open-cell foams, Chem.l Eng. J. 315 (2017) 608–620.

[21] K. Boomsma, D. Poulikakos, Y. Ventikos, Simulations of Flow through Open Cell Metal Foams Using an Idealized Periodic Cell Structure, Int. J. Heat Mass Tran. 24 (2003) 825-834. doi:10.1016/j.ijheatfluidflow.2003.08.002.
[22] A. Inayat, H. Freund, T. Zeiser, W. Schwieger, Determining the specific surface area of ceramic foams: The tetrakaidecahedra model revisited, Chem. Eng. Sci. 66 (2011) 1179–1188. doi:10.1016/j.ces.2010.12.031.
[23] M. Klumpp,A. Inayat, J. Schwerdtfeger,W. Schwieger, Periodic open cellular structures with ideal cubic cell geometry: Effect of porosity and cell orientation on pressure drop behavior, The Chemical Engineering Journal, 242 (2014) 364–378.
[24] P. Habisreuther, N. Djordjevic, N. Zarzalis, Statistical distribution of residence time and tortuosity of flow through open-cell foams, Chem. Eng. Sci. 64 (2009) 4943–4954. doi:10.1016/j.ces.2009.07.033.
[25] A. Della Torre, F. Lucci, G. Montenegro, A. Onorati, P. Dimopoulos Eggenschwiler, E. Tronconi, G. Groppi, CFD modeling of catalytic reactions in open-cell foam substrates, Comput. Chem. Eng. 92 (2016) 55–63. doi:10.1016/j.compchemeng.2016.04.031.
[26] C. Hutter, A. Zenklusen, S. Kuhn, P. Rudolf von Rohr, Large eddy simulation of flow through a streamwise-periodic structure, Chem. Eng. Sci. 66 (2011) 519–529. doi:10.1016/j.ces.2010.11.015.
[27] J.R. Tumbleston, D. Shirvanyants, N. Ermoshkin, R. Janusziewicz, A.R. Johnson, D. Kelly, K. Chen, R. Pinschmidt, J.P. Rolland, A. Ermoshkin, E.T. Samulski, J.M. DeSimone, Continuous liquid interface production of 3D objects, Science (80-. ). 347 (2015) 1349–1352. doi:10.1126/science.aaa2397.
[28] X. Zheng, H. Lee, T.H. Weisgraber, M. Shusteff, J. DeOtte, E.B. Duoss, J.D. Kuntz, M.M. Biener, Q. Ge, J.A. Jackson, S.O. Kucheyev, N.X. Fang, C.M. Spadaccini, Ultralight, ultrastiff mechanical metamaterials, Science (80-. ). 344 (2014) 1373–1377. doi:10.1126/science.1252291.
[29] C. Parra-Cabrera, C. Achille, S. Kuhn, R. Ameloot, 3D printing in chemical engineering and catalytic technology: structured catalysts, mixers and reactors, Chem. Soc. Rev. (2017) 1–35. doi:10.1039/C7CS00631D.
[30] L. Murr, S. Gaytan, F. Medina, E. Martinez, J.L. Martinez, D. Hernandez, B.I. Machado, D.A. Ramirez, R.B. Wicker, Characterization of Ti--6Al--4V open cellular foams fabricated by additive manufacturing using electron beam melting, Mat. Sci. Eng. A 572 (7-8) (2010) 1861-1868. doi:10.1016/j.msea.2009.11.015.
[31] A. Ortona, C.D'Angelo, S. Gianella, D. Gaia, Cellular ceramics produced by rapid prototyping and replication, Mater. Lett. 80 (2012) 95–98. doi:10.1016/j.matlet.2012.04.050.
[32] O. Santoliquido, G. Bianchi, P. Dimopoulos Eggenschwiler, A. Ortona, Additive manufacturing of periodic ceramic substrates for automotive catalyst supports, Int. J. Appl. Ceram. Technol. 14 (2017) 1164–1173. doi:10.1111/ijac.12745.
[33] B. Mueller, Additive Manufacturing Technologies – Rapid Prototyping to Direct Digital Manufacturing, Assem. Autom. 32 (2012). doi:10.1108/aa.2012.03332baa.010.
[34] T. Chartier, C. Dupas, M. Lasgorceix, J. Brie, E. Champion, N. Delhote, C. Chaput, Additive manufacturing to produce complex 3D ceramic parts, J. Ceram. Sci. Technol. 6 (2015) 95–104. doi:10.4416/JCST2014-00040.
[35] R.M. Ferrizz, J.N. Stuecker, J. Cesarano, J.E. Miller, Monolithic Supports with Unique Geometries and Enhanced Mass Transfer, Ind. Eng. Chem. Res. 44 (2005) 302–308. doi:10.1021/ie049468r.
[36] J.N. Stuecker, J.E. Miller, R.E. Ferrizz, J.E. Mudd, J. Cesarano, Advanced Support Structures for Enhanced Catalytic Activity, Ind. Eng. Chem. Res. 43 (2004) 51–55. doi:10.1021/ie030291v.
[37] S.L. City, R. Menon, S.L. City, R.U.S.A. Data, P. Classification, ( 19 ) United States ( 12 ), 1 (2014).
[38] A.C.A. Grande, J. Dubois, J.C.P. Camblor, Ø. Vistad, Additive manufacturing□: haute couture for chemical industries, (n.d.).
[39] P. Dimopoulos Eggenschwiler, V. Papetti, F. Lucci, A. Ortona, Additive Manufactured Open Cell Structures: Promising substrates for utomotive catalysts, Proceedings of the 18. Internationales Stuttgarter symposium, (2018).
[40] L. Giani, C. Cristiani, G. Groppi, E. Tronconi, Washcoating method for Pt/γ-$Al_2O_3$ deposition on metallic foams, Appl. Catal. B Environ. 62 (2006) 121–131. doi.org/10.1016/j.apcatb.2005.07.003.
[41] V- Meille, Review on methods to deposit catalysts on structured surfaces, Appl. Catal. A: General, 315 (2006) 1-17.
[42] A.F. Pérez-Cadenas, F. Kapteijn, J. A. Moulijn, Tuning the morphology of monolith coatings,

Appl. Catal. A: General, 319 (2007) 267-271.
[43] Z. Lv, T. Zhang, D. Jiang, J. Zhang, Q. Lin, Aqueous tape casting process for SiC, Ceram. Int.,35 (2009) 1889-1895.
[44] A. Cybulski, J. Moulijn, Monoliths in heterogeneous catalysis, Catal. Rev. – Sci. Eng. 36 (1994) 179–270.
[45] J. von Rickenbach, F. Lucci, C. Narayanan, P. Dimopoulos Eggenschwiler, D. Poulikakos, Effect of washcoat diffusion resistance in foam based catalytic reactors, Chem. Eng. J. 276 (2015) 388–397. doi:10.1016/j.cej.2015.03.132.
[46] Incropera, F. P.; DeWitt, D. P. Introduction to Heat Transfer; Wiley: New York, 1996.
[47] F. Patcas, G. Garrido, B. Kraushaar-Czarnetzki, CO oxidation over structured carriers: a comparison of ceramic foams, honeycombs and beads, Chem. Eng.Sci. 62 (15) (2007) 3984–3990.

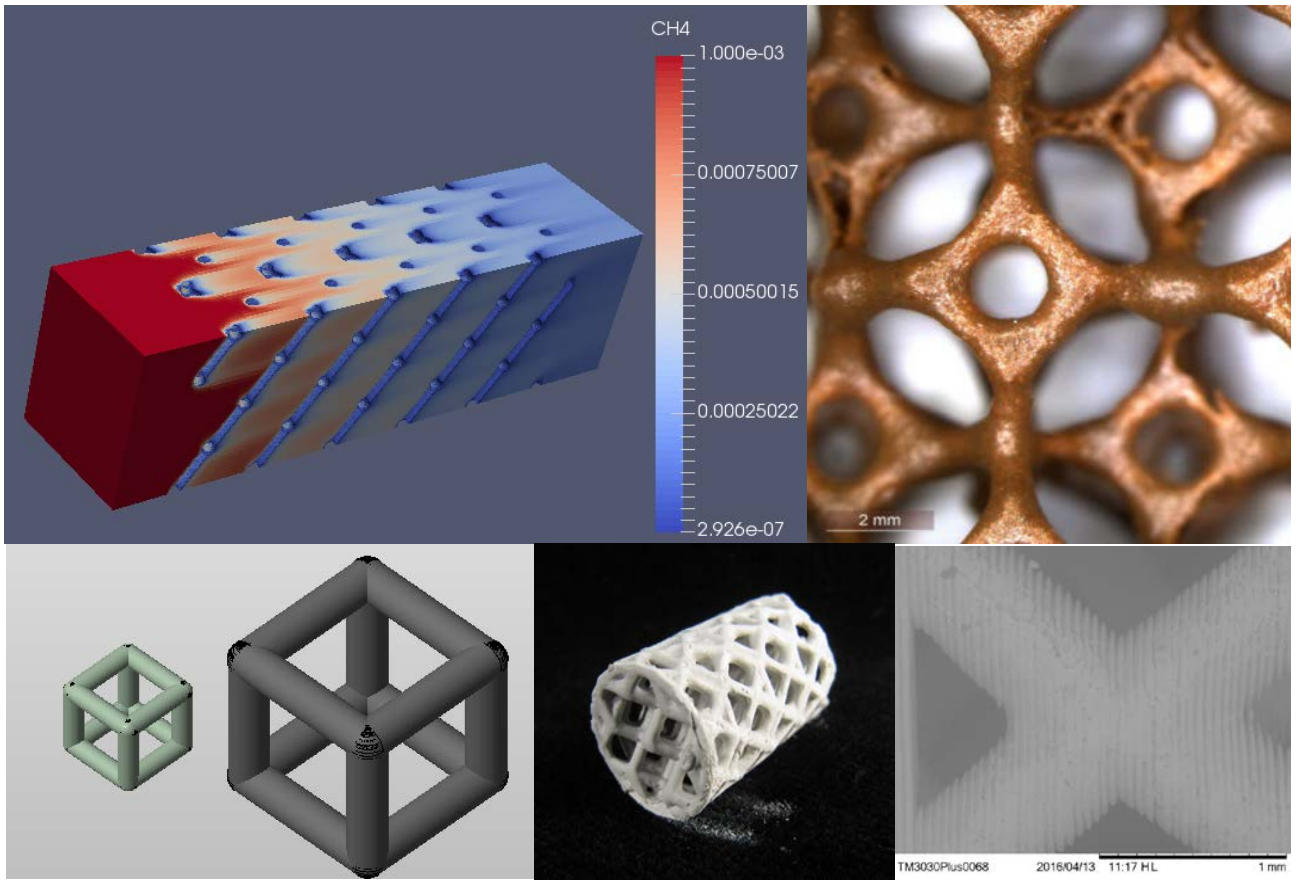
CH4
1.000e-03
0.00075007
0.00050015
0.00025022
2.926e-07
2 mm
TM3030Plus0068
2016/04/13 11:17 HL
1 mm